

Heterogeneous & Homogeneous & Bio- & Nano-

CHEMCATCHEM

CATALYSIS

Accepted Article

Title: Assessing inter and intra-particle heterogeneity in alumina-poor H-ZSM-5 zeolites.

Authors: Koen Kennes, Coralie Demaret, Jordi Van Loon, Alexey A.V. Kubarev, Guillaume Fleury, Michel Sliwa, Olivier Delpoux, Sylvie Maury, Bogdan Harbuzaru, and Maarten B.J. Roefsaers

This manuscript has been accepted after peer review and appears as an Accepted Article online prior to editing, proofing, and formal publication of the final Version of Record (VoR). This work is currently citable by using the Digital Object Identifier (DOI) given below. The VoR will be published online in Early View as soon as possible and may be different to this Accepted Article as a result of editing. Readers should obtain the VoR from the journal website shown below when it is published to ensure accuracy of information. The authors are responsible for the content of this Accepted Article.

To be cited as: *ChemCatChem* 10.1002/cctc.201700696

Link to VoR: <http://dx.doi.org/10.1002/cctc.201700696>

WILEY-VCH

www.chemcatchem.org



COMMUNICATION

Assessing inter and intra-particle heterogeneity in alumina-poor H-ZSM-5 zeolites.

Koen Kennes,^[a] Coralie Demaret,^[b] Jordi Van Loon,^[a] Alexey V. Kubarev,^[a] Guillaume Fleury,^[a] Michel Sliwa,^[c] Olivier Delpoux,^[b] Sylvie Maury^[b], Bogdan Harbuzaru,^[b] Maarten B.J. Roefsaers^{*[a]}

Abstract: In this report, we reveal the presence of significant variations in Brønsted catalytic activity within and between individual H-ZSM-5 zeolite crystals. Fluorescence microscopy in combination with a fluorogenic probe was used to resolve the catalytic activity at the nanoscale. The observed variations in catalytic activity could be directly linked to structural parameters and crystal morphology observed in scanning electron microscopy and by specifically staining crystal defects. The obtained results are directly compared with ensemble averaged information from techniques such as pyridine IR spectroscopy and nitrogen physisorption, typically used to characterize acid zeolites. The inter- and intra-particle heterogeneities resolved by the employed fluorescence approach remain unaddressed by bulk characterization. Our experimental results relate the heterogeneous catalytic activity to variation in both the Si/Al ratio and mesoporosity induced during the zeolite synthesis.

The preparation of zeolite-based industrial catalysts usually involves mixing the zeolites with silica and or alumina binders in order to dilute the zeolite properties and to obtain the desired throughput.^[1–3] During this process it is assumed that the zeolite crystals themselves are homogeneous in nature,^[2,4,5] i.e. only small variations in properties between the zeolite crystals in a batch exist. However, if this assumption is wrong and large variations in, for example, acid site density are present, parts of the shaped catalyst could become more active than others, resulting in undesired coke formation and thus a loss in catalyst activity and lifetime.^[4,6,7]

Two parameters impacting catalyst activity are the number and strength of acid sites present in a zeolite. These are directly related to the framework Al content,^[8,9] hence Al determination is often used to assess zeolite acidity. Several techniques can be

used to determine the Si/Al ratio, yielding powder averaged information, e.g. elemental analysis using inductive coupled plasma (ICP),^[10,11] magic angle spinning (MAS) ²⁹Si and ²⁷Al NMR^[8,12] laser induced break down spectroscopy (LIBS),^[13] X-ray photon electron spectroscopy (XPS)^[12,14] and time of flight-secondary ion mass spectrometry (TOF-SIMS).^[15,16] All of these techniques lead to the determination of the 'bulk' scale acidity and some are even able to obtain single crystal information given that crystal sizes and aluminum content are sufficiently large,^[17] e.g. single crystal X-ray diffraction^[17,18] and energy dispersive X-ray spectroscopy (EDX) coupled to electron microscopy potentially with focused-ion-beam milling.^[14,19] In summary, the acidic properties of zeolites are often deduced indirectly from the aluminum content. Further, no information regarding site accessibility is obtained in these results. Direct measurements of acid site density and strength are possible via temperature programmed desorption (TPD)^[8,14,20] and infrared-^[2,21,22] or Raman spectroscopy^[23] using basic probe molecules such as pyridine.^[2,24,25] The last two techniques also have the added benefit to distinguish Lewis and Brønsted sites. Even though they are mostly performed at the powder level, infrared and Raman spectroscopy can be performed in a microscopy setup yielding single crystal information.^[23] However, such measurements are typically hampered due to the low signal strengths, limiting their applicability to materials with rather high amounts of acid sites and in case of IR, a very limited spatial resolution (~300 nm) is attained limiting measurements to idealized single crystals.

Alternatively, fluorescence microscopy, combined with fluorogenic probe molecules, enables the localization of single catalytic turnovers, and thus the location of accessible Brønsted acid sites, with up to 20 nanometer resolution. By accumulating these turnovers into catalytic activity maps, as done in nanometer accuracy by stochastic chemical reactions (NASCA) microscopy, the catalyst performance can be assessed at the nanoscale.^[15,23,26–29] Hence, such measurements directly reveal the combined effect of acidity and accessibility, as these stochastic catalytic turnovers are localized while occurring on accessible acid sites.

In this report, the Brønsted acid-catalyzed oligomerization of furfuryl alcohol (FFA) was used to probe the accessibility of Brønsted acid sites in a commercial batch of H-ZSM-5 zeolite crystals. NASCA microscopy revealed large inter- and intraparticle heterogeneities in the activity maps which were previously unresolved by bulk measurements. In addition to NASCA microscopy, catalysts stained with dedicated probe molecules were studied with confocal laser-scanning microscopy (CLSM). By combining these two fluorescence microscopy approaches with structural characterization by scanning electron microscopy (SEM), the existence of different types of crystals

[a] K. Kennes, J. Van Loon, A. V. Kubarev, G. Fleury, M. B. J. Roefsaers

Centre for Surface Chemistry and Catalysis
Faculty of Bioscience Engineering
KU Leuven
Kasteelpark Arenberg 23, 3001 Heverlee (Belgium)
E-mail: maarten.roefsaers@biw.kuleuven.be

[b] C. Demaret, O. Delpoux, S. Maury, B. Harbuzaru
IFP Energies nouvelles
Lyon Establishment
Rond point de l'échangeur de Solaize – BP-3
69360 Solaize, France

[c] M. Sliwa
Laboratoire de Spectrochimie Infrarouge et Raman - LASIR
CNRS, UMR 8516
Univ. Lille
F-59000 Lille, France

Supporting information for this article is given via a link at the end of the document.

COMMUNICATION

within the powdered batch is revealed. Differences in mesoporosity as well as the Si/Al ratio originating from the synthesis are exposed as the source of the heterogeneity.

To assess the catalytic performance of individual H-ZSM-5 crystals the transient fluorescence signal generated upon formation of fluorescent oligomers were recorded. This fluorescence signal enables to localize single catalytic turnovers precisely. Accumulation of these turnover positions in $50 \times 50 \text{ nm}^2$ bins straightforwardly reveals the local catalytic performance. When such activity maps are combined with structural information from SEM, a detailed correlation between crystal activity and structure is obtained. Figure 1 shows such an SEM image (A) and the corresponding activity map (B). The false color scale indicates the number of turnovers within each bin. A quick look at these images already shows that there are at least three types of crystals within this powdered catalyst batch. The first group consists of crystals with a high catalytic activity homogeneously distributed throughout the crystal. A second group consists of particles with reactivity concentrated near the outer rim of the crystals and almost no observable activity in the center. The third group of crystals shows almost no activity at all. By correlating these catalytic activity maps to the crystal morphology revealed by SEM, it becomes apparent that crystals with a rough surface mostly belong to the first group of highly active H-ZSM-5 particles (Figure 1C, D). Further, particles with a smooth surface are much less active and belong to the second and third group, only showing activity at the particle exterior or not showing measurable activity at all. Figure S1 shows a magnified view on the three types of crystals. Such large differences in catalytic activity can be explained by either a variation in acid site density and strength or by differences in accessibility of acid sites e.g. due to the presence of extra-framework porosity, which induces surface roughness.^[30]

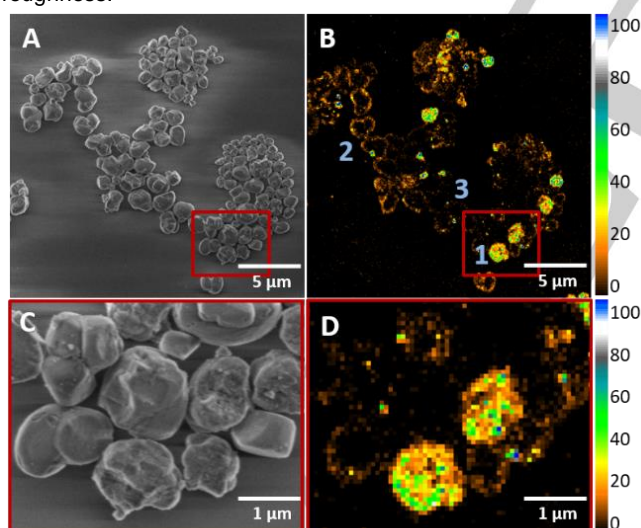


Figure 1. SEM image (A) and NASCA activity map (B) of H-ZSM-5 zeolites. C and D are enlargements of the areas indicated in A and B respectively. In B, the three types of crystals are indicated: 1: crystals with a homogeneous activity, 2: crystals where only the edge is active and 3: crystals that show almost no activity. The colour scale represents the normalized detected reaction rate per bin ($50 \times 50 \text{ nm}^2$).

Hence, a straightforward explanation would be that the rough appearing crystals contain a significant amount of additional porosity which enhances the molecular transport, while reactions in the smooth surface crystals experience diffusion limitations limiting the reactivity in the time scales used in the NASCA experiments.

This hypothesis can be verified by increasing the reaction time, in order to ensure the FFA molecules have sufficient time to diffuse throughout the whole crystals. If the discrepancy in reactivity observed originates from mass transfer limitation, such experiments should lead to a more homogeneous activity within the particles. Since the duration of NASCA microscopy measurements is limited due to inevitable built-up of fluorescence background, confocal fluorescence microscopy was used to study catalytically stained zeolite crystals. Therefore, in order to test for the presence of these diffusion limitations, we catalytically stained the zeolite sample. Specifically, FFA ($20 \mu\text{l}$) was added to an aqueous H-ZSM-5 suspension (10 mg/ml) and left to react for 24 hours at room temperature. Figure 2 shows the optical transmission (A) and the corresponding confocal fluorescence (B) images of the H-ZSM-5 zeolites after FFA oligomerization. As was previously observed in the correlated NASCA experiments, these measurements clearly confirm large variations in catalytic activity of the $\sim 1\text{-}2 \mu\text{m}$ crystals; several crystals show a high fluorescence intensity while others only display poor to no measurable fluorescence. A 3D confocal stack (see Supporting information) was recorded and used to obtain the average activity per particle. These results are plotted in Fig. 2D and clearly reveal the presence of at least three different populations in this powdered batch, as three Lorentzians are minimally needed to obtain a satisfactory fit for the distribution plot (see Table S1 for the details of the plot and the corresponding fit). This agrees with the fact that we observe three different NASCA reactivity maps.

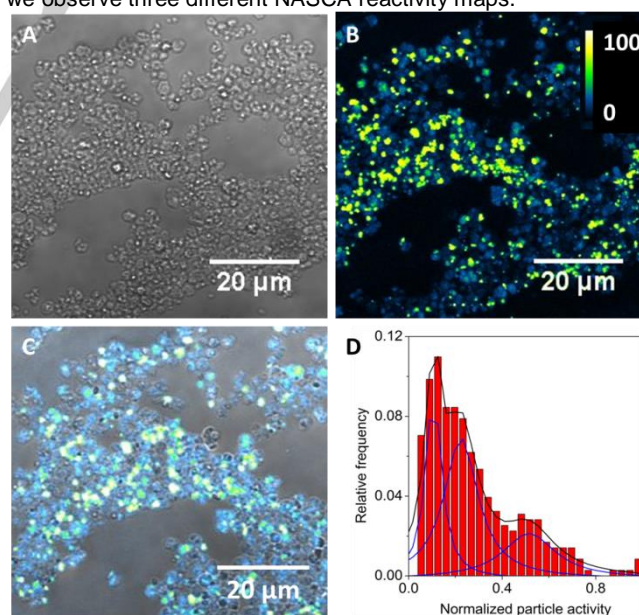


Figure 2. Transmission image (A) and 3D projection of a Z-stack (B) of 10 confocal images ($0\text{-}10 \mu\text{m}/0.25 \mu\text{m}$) of ZSM-5-507 zeolites after FFA reaction. The color scale indicates the normalized intensity. The correlated image of A and B (C) and a histogram of the normalized particle activity (D). The blue lines represent the Lorentzian fits, the black line is the sum of the three Lorentzians.

COMMUNICATION

The longer reaction time compared to the NASCA measurements, which are performed directly after addition of the fluorogenic reagent, show that mass transport limitations are not the cause of the differences in catalytic activity as H-ZSM-5 zeolites have been shown to be fully accessible towards the FFA oligomerization.^[15,31] Therefore, it must be concluded that a variation in the amount of Brønsted acid sites is causing the differences in activity inside and between individual zeolite crystals. In order to confirm the correlation between particle morphology and activity, the H-ZSM-5 particles stained with FFA during 24h were additionally investigated using an integrated (wide field) fluorescence and scanning electron microscope (iFLEM). To avoid beam-damage of the fluorescent reaction products, first the wide-field fluorescence images were recorded followed by SEM imaging. These measurements confirmed the earlier observations that the crystals with a rough surface are generally more active than those with an apparent smooth surface (Figure S2).

Interparticle variations in Brønsted acidity can account for the variation in catalytic performance they however do not explain the differences in crystal appearance in SEM. The observed surface roughness could be an indication of particle imperfections and the presence of defects and extra-framework porosity.^[30] To visualize the extra-framework porosity with the same amount of detail, we specifically stained the accessible pore-mouths of the straight microporous ZSM-5 channels using a large fluorescent molecule, i.e. 4-(4-diethylaminostyryl)-N-methylpyridinium iodide (DAMPI).^[31] DAMPI is practically non-fluorescent in solution due to cis-trans isomerization of the dye backbone, which is prevented when adsorbed inside the entrances of the H-ZSM-5 micropores. However, due to the size of the diethylamino group DAMPI cannot enter the internal micropores. Figure 3 (and Figures S3-S5) shows several representative confocal fluorescence images (C and D) of DAMPI-stained H-ZSM-5 crystals with their corresponding SEM images (A and B). These measurements show that for crystals with a smooth surface DAMPI fluorescence is restricted to the outer surface indicating a lack of extra-framework porosity and defects. On the other hand, most of the rough crystals are stained throughout indicative for a high degree of extra-framework porosity. Note that for some crystals with a rough surface appearance in SEM the DAMPI fluorescence is also restricted to the outer surface (Figure S5). The crystal in Figure S5 shows that these are in fact two (or more) intergrown crystals, one with a smooth surface that is partially overgrown by one with a rough appearance. The presence of extra-framework porosity was also confirmed by transmission electron microscopy. Figure S6 shows the TEM images of two different crystals from this batch. Whereas the first crystal exhibits very little mesoporosity, which is in line with DAMPI staining being restricted to the outer surface, the second crystal shows an extensive network of large mesopores (10-20 nm), which could be related to crystals that show a complete DAMPI staining. While it proved practically difficult to correlate these TEM observations to the observed surface appearance in SEM, the results clearly support our earlier observations. Nitrogen physisorption experiments (Figure S7) also support the presence of a small amount of mesopores of about 25 nm that could be related to these rough particles, but this bulk technique obviously fails to reveal the location and distribution of these pores inside the crystals.

Although, no specific information was received regarding the preparation of this H-ZSM-5 sample by the supplier, Zeolyst International, the observed differences in crystal morphology, and activity could originate both from the zeolite synthesis as well as from post-synthetic treatment. As for the latter, an (un)intentional dealumination can occur either during the calcination step or during a post-synthetic treatment via acid leaching or steaming. Such dealumination enhances the molecular transport via the introduction of mesopores as aluminum is removed from the framework structure. In a previous study^[15] the effect of dealumination via mild steaming on large (20 x 20 x 100 μm^3) H-ZSM-5 zeolites was shown to increase surface porosity and alter the aluminum distribution throughout the entire crystal, which resulted in an enhanced accessibility and reactivity. However, the observed structure-activity distribution in this H-ZSM-5 conflicts with the expected behavior. Indeed, the smooth crystals show the least amount of activity; if this low activity is caused by a dealumination and a reduced amount of acid sites, they should also contain the highest degree of accessibility through the incorporation of extra-framework porosity which is not observed in the DAMPI experiments. Furthermore, based on their morphology one could expect that the smooth crystals are intact rather than dealuminated.

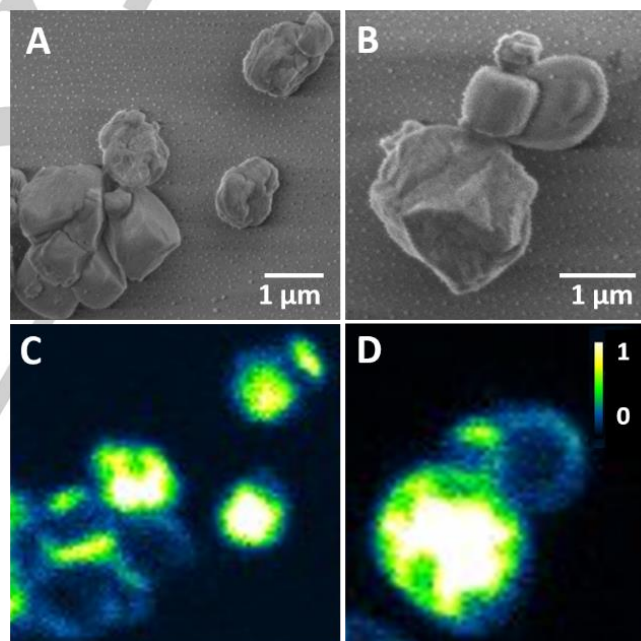


Figure 3. A) and B) SEM images of DAMPI-stained H-ZSM-5 crystals and C) and D) their respective confocal images.

Hence, an alternative explanation could be that the rough and smooth particles are actually two different crystal types formed during the synthesis. During the nucleation step and initial growth a silica rich 'precursor' is typically obtained, further growth slowly increases the aluminum content with a gradient towards the rim, a process well-known for ZSM-5 as aluminum zoning.^[32] Hence, zoning of aluminum, specifically in alumina-poor zeolites, leads to crystals with very little aluminum, and therefore very low catalytic activity, in the core, but more aluminum, and thus more activity, at the rim. This is in line with the performance of many of

COMMUNICATION

the smooth-surfaced crystals (type 2). Particles showing no activity at all (type 3) would in this case correspond to zeolites with overall very low aluminum content; note that crystal-to-crystal variations in as-synthesized zeolites have been reported before.^[33,34] Crystals of type 1, with the highest activity, should contain more aluminum and will have hence been formed at the later stages during the synthesis. This does not explain the presence of mesoporosity mainly in the aluminum richer (type-1) crystals. As these crystals must have formed during the later stages of the zeolite synthesis under depleted precursor concentrations they might intrinsically contain more defects, or these mesopores could be the result of dealumination, either unintentionally via (fast) calcination or deliberately introduced via post-synthetic dealumination. The fact that 18% of the rough-surfaced crystals do not display high catalytic activity is supportive for the post-synthetic dealumination known to induce severe interparticle heterogeneity.^[23]

Typical pyridine IR measurements (Figure S8) show a total of 11 $\mu\text{mol/g}$ Brønsted acid sites of which 8 $\mu\text{mol/g}$ are weak and 3 $\mu\text{mol/g}$ are medium weak acid sites. Note that this is about 1/3 of what could theoretically be expected for this Si/Al ratio, however this specific sample is already testing the sensitivity limits of the used bulk measurement with 20 g of sample. This routinely employed characterization also does not uncover inter- or intraparticle heterogeneity.

Direct mapping of the exact aluminum distribution would provide additional evidence for the proposed mechanism. However, given the small crystal size and the low aluminum content such measurements cannot be performed with techniques typically used to map elemental composition such as SEM-EDX.

In conclusion, several fluorescence microscopy techniques were used to probe the accessible Brønsted acid sites in individual aluminum poor H-ZSM-5 crystals from a commercial batch. Reactivity maps constructed using the super-resolution technique NASCA microscopy revealed large inter- and intraparticle heterogeneities that are unaddressed using conventional bulk techniques such as pyridine IR measurements. Based on the nanoscale activity maps, three types of crystals could be identified inside the zeolite batch: (1) crystals with homogeneous high catalytic activity, (2) crystals with highly active shell and inactive core and (3) crystals that do not display significant activity. Correlated SEM imaging showed a strong relation with the crystal surface morphology. Rough surfaced zeolite crystals are typically more active. Pre-staining with FFA and DAMPI leads us to conclude that this batch of zeolites contained two different populations of zeolite crystals after synthesis. More generally, we conclude that when significant interparticle structural differences are observed via electron microscopy, as is often the case in catalytic research,^[33] they can be an indication of heterogeneity in catalytic activity and suboptimal catalysts performance. However, as traditional catalytic activity assessment techniques are not able to resolve such small scale heterogeneity, this indication is often ignored, while in combination with the right microscopic tools it can be used to optimize the catalysts.

Experimental Section

Zeolites samples

The H-ZSM-5 zeolite crystals with a silicon to aluminum ratio of 507 were purchased from Zeolyst International and were calcined at 450°C before use. The corresponding XRD diffractogram is shown in figure S9.

Sample preparation for NASCA experiments

The cover slides (22 x 22 mm, #1) used as the substrate in the experiments are calcined at 500 °C and treated in an ozone reactor (Ultra violet products, PR-100), before the sample is spin coated (60 s 3000 rpm) from a 10 mg H-ZSM-5-507 (Zeolyst International, CBV 10002) in 10 ml Milli Q (Synergy UV, Merck Millipore) water suspension. Subsequently, the cover slides containing sample are calcined in a muffle furnace (Nabertherm LVT 3/11) to remove any organic contaminants. This calcination is performed using a specified heating program in order to minimize alterations to the sample. First, the sample is slowly heated from room temperature to 80 °C. This temperature is held for 1 hour, after which the sample is further heated to 120 °C with a heating ramp of 1 °C / min. Again, this temperature is held for 1 hour, after which the temperature is further increased at 1 °C / min to 450 °C, where it remains for at least 48 hours. When commencing the experiments, the sample was freshly taken from the muffle furnace in order to prevent unwanted contamination.

Integrated light and electron microscope

In order to enable a straightforward correlation of scanning electron microscopic structural information with single catalytic turnover activity maps, an integrated light and electron microscope was applied in this research. This integrated system is based on a FEI Quanta 250 FEG environmental scanning electron microscope in which the original SEM door is replaced by the SECOM platform acquired from Delmic BV. Most importantly, the SECOM platform comprises a sample stage, capable of holding a high numerical aperture oil-immersion objective lens (Nikon plan APO VC 100x, 1.4 NA), and an optically transparent window that allows excitation and fluorescence light to be coupled into and out of the vacuum SEM chamber. This configuration makes it possible to obtain structural images from the top of the sample and to consecutively perform single turnover mapping from the bottom side. The latter is achieved by using excitation light at 532 nm provided by an Omicron Laserhub, which is guided towards the objective lens by means of a 442/532 nm dichroic mirror and fluorescence being filtered out before detection with a 542 nm long pass filter. The vacuum conditions in the sample chamber during SEM imaging, prior to the NASCA experiments, demands a vacuum compatible immersion oil, i.e. 1-Ethyl-3-methylimidazolium acetate (BASF). An EMCCD camera (Hamamatsu C9100-23B, 512 x 512 pixels) is positioned on the outside of the SEM door to detect the emitted fluorescence signal. The optical pathway in our specific system differs from the standard SECOM platform, as it was optimized for single molecule detection.

Correlative structure activity mapping using the integrated light and electron microscope

Correlative structural and NASCA imaging is performed by a predetermined set of experimental steps. Initially, the cover slides containing the sample are mounted on the sample stage of the

COMMUNICATION

integrated light and electron microscope, after which the SEM chamber is brought to vacuum. At this point, SEM imaging is performed. After acquiring the necessary structural images of the sample, the microscope is brought back to atmospheric pressure and a perfusion chamber is added onto the cover slide (PC8R-1.0-CoverWell, Grace Bio labs), in which 50 μ l of a 1.73 M furfuryl alcohol in Milli Q water solution is added. After adding the fluorogenic reagent solution, 10.000 frame movies are acquired using the EMCCD camera set at 30 ms exposure time and 297 EM gain, to perform single catalytic turnover detection.

NASCA analysis

The acquired single turnover movies are properly analyzed using the localizer software for Igor Pro (Wavemetrics). This software is available online (<https://bitbucket.org/pdedecker/localizer>) and is applied to localize the individual turnovers and accumulate them into the NASCA activity maps. As such, the activity maps contain all turnovers that occurred over the course of the movie and within the focal plane in the middle of the crystals. After the turnovers were accumulated, identical emitters in consecutive frames were removed by consolidation.

Fluoview experiments

The CLSM used in the performed experiments is an Olympus IX81, equipped with a laser combiner, providing 532 nm continuous excitation light, and a 100X 1.4 NA objective lens. Fluorescence detection is achieved using a PMT. The excitation light was filtered using a 535 nm dichroic mirror and a 545 nm long pass filter. The zeolites were added to a solution of 1.73 M FFA in Milli Q for 24 hours or to a solution of 2 mM of DAMPI for 24 hours before being spin coated in a glass cover slide (2000 rpm for 1 min). Separate confocal images were taken every 0.25 μ m for a total depth of 10 μ m (41 images) for 512 by 512 pixels. The program image-J was used to construct a 3D image of these images. The provided 3D-object localizer was used to calculate the average particle intensity of each particle.

Nitrogen physisorption

Nitrogen physisorption isotherms were collected at 77 K using a MicroMeritics 3Flex instrument. The samples were evacuated at 200°C for 12 h prior to measurement. The pore size distributions were obtained using the BJH method applied to both the adsorption and the desorption branches.

Pyridine infrared experiments

The pyridine infrared measurements were performed in transmission mode using a Nexus-1 (ThermoOptek Nicolet) spectrometer. 64 scans were performed. Before measuring the samples were dried in an oven at 450°C for 10 hours. The measurements were performed at 150°C after 2 hours, 250°C, 350°C and 450°C after 1 hour each.

Acknowledgements

The authors acknowledge financial support from the Research Foundation-Flanders (FWO, G.0962.13), KU Leuven Research Fund (C14/15/053, OT/12/059), the Hercules foundation

(HER/11/14). The research leading to these results has received funding from the European Research Council under the European Union's Seventh Framework Programme (FP/2007-2013)/ERC Grant Agreement no. [307523], ERC-Stg LIGHT to M.B.J.R.

Keywords: super-resolution fluorescence microscopy • electron microscopy • meso/macropores • zeolites • acidity

- [1] N. Michels, S. Mitchell, J. Pe, *ACS Catal.* **2014**, *4*, 2409.
- [2] P. Pe, A. Ateka, D. Marta, T. Aguayo, J. Bilbao, **2016**.
- [3] C. Sprung, B. M. Weckhuysen, **2014**, 3667.
- [4] L. Itani, V. Valtchev, J. Patarin, S. Rigolet, F. Gao, G. Baudin, *Microporous Mesoporous Mater.* **2011**, *138*, 157.
- [5] C. Li, Z. Wu, *Handb. Zeolite Sci. Technol.* **2003**.
- [6] T. Ma, S. P. Mu, B. Kraushaar-czarnetzki, **2001**, 2573.
- [7] G. T. Whiting, A. D. Chowdhury, R. Oord, P. Paalanen, B. M. Weckhuysen, *Faraday Discuss.* **2016**, *188*, 369.
- [8] G. H. Kuehl, H. K. C. Timken, *Microporous Mesoporous Mater.* **2000**, *35–36*, 521.
- [9] P. Payra, P. K. Dutta, *ChemInform* **2004**, *35*, 1.
- [10] J. Aguilera-Sigalat, D. Bradshaw, *Coord. Chem. Rev.* **2015**.
- [11] M. C. Alonso, L. Trapiella-Alfonso, J. M. C. Fernández, R. Pereiro, A. Sanz-Medel, *Biosens. Bioelectron.* **2016**, *77*, 1055.
- [12] D. Fodor, F. Krumeich, R. Hauert, J. A. Van Bokhoven, *Chem. A Eur. J.* **2015**, *21*, 6272.
- [13] M. Hornackova, M. Horňáček, J. Rakovský, P. Hudec, P. Veis, *Spectrochim. Acta - Part B At. Spectrosc.* **2013**, *88*, 69.
- [14] E. Kolobova, A. Pestryakov, G. Mamontov, Y. Kotolevich, N. Bogdanchikova, M. Farias, A. Vosmerikov, L. Vosmerikova, V. Cortes Corberan, *Fuel* **2017**, *188*, 121.
- [15] Z. Ristanovic, J. P. Hofmann, G. De Cremer, A. V. Kubarev, M. Rohnke, F. Meirer, J. Hofkens, M. B. J. Roeflaers, B. M. Weckhuysen, *J. Am. Chem. Soc.* **2015**, *137*, 6559.
- [16] K. Norrman, A. Ghanbari-Siahkali, N. B. Larsen, *Annu. Rep. Prog. Chem., Sect. C: Phys. Chem.* **2005**, *101*, 174.
- [17] S. man. Seo, O. S. Lee, H. S. Kim, D. H. Bae, I.-J. Chun, W. T. Lim, *Bull. Korean. Chem. Soc.* **2007**, *28*, 1675.
- [18] M. Usman, S. Mendiratta, S. Batjargal, G. Haider, M. Hayashi, N. Rao Gade, J.-W. Chen, Y.-F. Chen, K.-L. Lu, *ACS Appl. Mater. Interfaces* **2015**, 151006130502006.
- [19] A. Sartbaeva, N. H. Rees, P. P. Edwards, A. J. Ramirez-Cuesta, E. Barney, *J. Mater. Chem. A* **2013**, *1*, 7415.
- [20] L. Shirazi, E. Jamshidi, M. R. Ghasemi, *Cryst. Res. Technol.* **2008**, *43*, 1300.
- [21] D. M. Roberge, H. Hausmann, W. F. Hölderich, *Phys. Chem. Chem. Phys.* **2002**, *4*, 3128.
- [22] D. Verboekend, A. M. Chabaneix, K. Thomas, J. P. Gilson, J. Perez-Ramirez, *CrystEngComm* **2011**, *13*, 3408.
- [23] K. L. Liu, A. V. Kubarev, J. Van Loon, H. Uji-I, D. E. De Vos, J. Hofkens, M. B. J. Roeflaers, *ACS Nano* **2014**, *8*, 12650.
- [24] X. Pu, N. Liu, L. Shi, *Microporous Mesoporous Mater.* **2015**, *201*, 17.

COMMUNICATION

- [25] A. B. Pinar, C. Márquez-Álvarez, M. Grande-Casas, J. Pérez-Pariente, *Proc. 5th Serbian-Croatian-Slovenian Symp. Zeolites* **32**.
- [26] Z. Ristanovic, M. M. Kerssens, A. V. Kubarev, F. C. Hendriks, P. Dedecker, J. Hofkens, M. B. J. Roefsaers, B. M. Weckhuysen, *Angew. Chemie - Int. Ed.* **2015**, *54*, 1836.
- [27] A. V. Kubarev, K. P. F. Janssen, M. B. J. Roefsaers, *ChemCatChem* **2015**, *7*, 3646.
- [28] K. P. F. Janssen, G. De Cremer, R. K. Neely, A. V. Kubarev, J. Van Loon, J. a Martens, D. E. De Vos, M. B. J. Roefsaers, J. Hofkens, *Chem. Soc. Rev.* **2014**, *43*, 990.
- [29] M. B. J. Roefsaers, G. De Cremer, J. Libeert, R. Ameloot, P. Dedecker, A. J. Bons, M. Bückins, J. A. Martens, B. F. Sels, D. E. De Vos, J. Hofkens, *Angew. Chemie - Int. Ed.* **2009**, *48*, 9285.
- [30] A. Silva, L. Miranda, M. Nele, B. Louis, M. Pereira, *Catalysts* **2016**, *6*, 30.
- [31] M. B. J. Roefsaers, R. Ameloot, M. Baruah, H. Uji-i, M. Bulut, G. De Cremer, U. Müller, P. A. Jacobs, J. Hofkens, B. F. Sels, D. E. De Vos, *J. Am. Chem. Soc.* **2008**, *130*, 5763.
- [32] N. Danilina, F. Krumeich, S. A. Castelanelli, J. A. Van Bokhoven, *J. Phys. Chem. C* **2010**, *114*, 6640.
- [33] S. Sang, F. Chang, Z. Liu, C. He, Y. He, L. Xu, *Catal. Today* **2004**, *93–95*, 729.
- [34] S. Narayanan, A. Sultana, Q. Thinh Le, A. Auroux, *Appl. Catal. A Gen.* **1998**, *168*, 373.

WILEY-VCH

Accepted Manuscript